S.T. Yau High School Science Award

Research Report

Investigating physical conditions and critical factors across the center of the galaxy M82

The Team
Name of team member: Valencia Zhang
School: Phillips Academy

Name of supervising teacher: Dr. Jakob den Brok
Job Title: Postdoctoral Fellow
School/Institution: Harvard & Smithsonian Center for Astrophysics

Commitments on Academic Honesty and Integrity

We hereby declare that we

1. are fully committed to the principle of honesty, integrity and fair play throughout the competition.
2. actually perform the research work ourselves and thus truly understand the content of the work.
3. observe the common standard of academic integrity adopted by most journals and degree theses.
4. have declared all the assistance and contribution we have received from any personnel, agency, institution, etc. for the research work.
5. undertake to avoid getting in touch with assessment panel members in a way that may lead to direct or indirect conflict of interest.
6. undertake to avoid any interaction with assessment panel members that would undermine the neutrality of the panel member and fairness of the assessment process.
7. observe the safety regulations of the laboratory(ies) where we conduct the experiment(s), if applicable.
8. observe all rules and regulations of the competition.
9. agree that the decision of YHSA is final in all matters related to the competition.

We understand and agree that failure to honour the above commitments may lead to disqualification from the competition and/or removal of reward, if applicable; that any unethical deeds, if found, will be disclosed to the school principal of team member(s) and relevant parties if deemed necessary; and that the decision of YHSA is final and no appeal will be accepted.

(Signatures of full team below)

X *Valencia Zhang*
Name of team member: Valencia Zhang

Name of supervising teacher: Dr. Jakob den Brok

Declaration of Academic Integrity

The participating team declares that the paper submitted is comprised of original research and results obtained under the guidance of the instructor. To the team's best knowledge, the paper does not contain research results, published or not, from a person who is not a team member, except for the content listed in the references and the acknowledgment. If there is any misinformation, we are willing to take all the related responsibilities.

Names of team members: Valencia Zhang

Signatures of team members: *Valencia Zhang*

Name of the instructor: Jakob den Brok

Signature of the instructor: 

Date: 8/24/2024

Investigating physical conditions and critical factors across the center of the galaxy M82

Valencia Zhang
Phillips Academy

Under the direction of
Dr. Jakob den Brok and Dr. Qizhou Zhang
Center for Astrophysics, Harvard & Smithsonian

August 24, 2024

Abstract

Stars, the fundamental building blocks of the Universe, are born in molecular clouds. In order to understand how they form and drive processes such as galaxy and planet formation, it is crucial to study the physical conditions of these clouds. However, this task is challenging and has only recently become possible with high resolution data collected at the star-forming. The galaxy Messier 82 (M82) is an ideal subject for molecular gas studies because of its close proximity to Earth, enhanced star formation activity, and brightness of line emission. Accordingly, we analyze high resolution millimeter emission from carbon monoxide (CO) and its isotopologues. We evaluate the molecular gas conditions in M82's center, including temperature, density, and CO-to-H_2 conversion factor, $\alpha_{\rm CO}$, using two non-local thermal equilibrium modeling approaches and likelihood analysis. Our first simpler approach assumes uniform conditions per sightline of gas, and the second, more sophisticated approach assumes a smoothly changing gas density. The gas conditions derived by the two models differed significantly. We find that the intensity ratio between the $J = 2 - 1$ lines of ^{12}CO and ^{13}CO, can be used as an observational tracer of $\alpha_{\rm CO}$. Overall, our results constrain the conditions of M82's gas, highlight the need for more sophisticated model prescriptions, and uncover a new observational tracer for the $\alpha_{\rm CO}$ in starburst galaxies.

keywords: star formation, molecular emission, starburst galaxies

Summary

Some of the most fundamental questions in astrophysics concern the origin and evolution of galaxies, planets, and life. As stars are the key building blocks of our Universe, it is critical to study their formation, which occurs when molecular gas clouds collapse. Analyzing the gas's temperature, density, and mass helps us better model and understand star formation.

Star-forming gas is primarily molecular hydrogen, which is not directly observable, but we can use emission of the second most abundant molecule, carbon monoxide (CO), instead. We model and compare CO emission from the Messier 82 galaxy, which is known for its enhanced star forming activity, with simulations that predict emission under various environments. We employ two approaches to explain the gas characteristics and find significantly different results. We compute the value of a factor which translates from CO emission to total gas mass. Importantly, we found a correlation between this factor and observed emission, allowing astronomers to directly compute the factor from observations and avoid complicated analysis. Overall, our work emphasizes the importance of caution when modeling molecular gas, the need for more models to accurately describe molecular gas conditions, and the discovery of a new observational tracer for the conversion factor.

1 Introduction

Stars are fundamental building blocks of the Universe, as they determine the structure, evolution, and luminosity of galaxies, and serve as cradles for planetary systems [1]. Understanding star formation thereby better informs our understanding of the development of galaxies, planets, and life.

1.1 The Role of Molecular Gas in Star Formation

Star formation is a crucial step in the life cycle of molecular gas. The space between stars in galaxies, known as the interstellar medium (ISM), is filled with molecular gas clouds [2]. Over time, these clouds cool and eventually collapse to form stars [3]. Despite significant efforts in the past decades, however, the specific physical mechanisms and properties by which molecular clouds affect the process and rate of star formation remain elusive [4]. Observations of the Milky Way and nearby galaxies show a correlation between molecular gas and star formation, suggesting that the conditions of the gas may regulate the process [5, 6, 7]. Thus, studies of molecular gas can provide crucial insights into star formation.

Extragalactic studies are especially valuable because they allow us to obtain a global environmental picture of the galaxy, unlike in the Milky Way, where we are limited to studying individual clouds [3]. Extragalactic targets also enable us to probe diverse conditions. For example, starburst galaxies, which resemble conditions in the early Universe, offer crucial insights into star formation history [8]. The potential to infer star formation mechanisms from nearby galaxies motivates the development of methods to observe and probe star-forming gas.

1.2 Observing and Analyzing Molecular Clouds

Star-forming molecular gas is primarily composed of molecular hydrogen (H_2). However, H_2 emission is not practically observable in star-forming conditions [9]: because hot gas opposes collapse, stars must form in cold gas, and such low temperatures are in turn too cold to excite the lowest energy levels of H_2 [10]. Consequently, we must turn to detectable proxies for H_2, such as molecular emission. The second most abundant molecule in the ISM after H_2 is carbon monoxide ($^{12}C^{16}O$, hereafter CO or ^{12}CO), which is formed when carbon and oxygen atoms combine. The CO molecule has multiple rotational energy levels denoted by the quantum number J that can be excited even in cold molecular clouds, making it a reliable tracer of H_2. Research has shown a direct relationship between the intensity of CO emission and H_2 mass through the critical CO-to-H_2 conversion factor [11].

While CO is an effective tracer of H_2 in Milky Way-like environments, it can be less effective in extreme star-forming environments due to optical depth effects [1]. Emission from the $J = 1$–0 transition of CO (also referred to as rotational line) is optically thick [12], leading to a degeneracy in gas conditions [9]. Thus, it is crucial to study optically thin emission, such as less abundant CO species with different isotopic compositions known as isotopologues. The $^{13}C^{16}O$ isotopologue (hereafter abbreviated as ^{13}CO) has a relatively low abundance ($CO/^{13}CO \sim 20 - 70$) and is generally optically thin [13]. Similarly, $C^{18}O$ is about 30 times less abundant than ^{13}CO and is optically thin [14]. The intensities of CO isotopologue energy transitions are particularly valuable because they can trace the entire column of gas.

Emission from CO isotopologues can be faint because of their low abundance, making observations difficult. Recent advances in instrumentation have enabled astronomers to obtain spatially resolved observations of CO emission, providing unique opportunities to see within galaxies beyond the Milky Way. With CO line emission data in hand, a common

[1] Optical depth describes a material's ability to block or absorb light; a larger optical depth corresponds to less transmitted radiant power through the material. Thus, as light passes through an optically thick medium, it is constantly absorbed and scattered, significantly reducing the detected intensity.

approach in literature is to assume the emitting gas satisfies Local Thermodynamic Equilibrium (LTE; cf., [15]) and solve the radiative transfer equation directly [16]. While this approach is straightforward, the LTE assumption is often incorrect for star-forming gas, and has been found to have inconsistencies with other methods [17]. Thus, a non-LTE approach is crucial.

1.3 Our Work

To date, no non-LTE modeling has been performed on high resolution CO emission from the starburst galaxy Messier 82 (M82). In this paper, we present high resolution observations of M82 and investigate the physical properties of its star forming gas under a non-LTE regime. This study is particularly exciting because we can resolve the molecular cloud structure of M82. In Section 2, we introduce our target and data. In Section 3, we explain our methods for fitting the observations, detailing two models: one assuming uniform emitting gas and the other assuming smoothly changing log-normal density. In Section 4, we present the main results. We discuss the interpretation of the results in Section 5, and conclude in Section 6.

We address two questions concerning the physical conditions of M82's molecular gas and how emission from CO isotopologues trace underlying variations in these gas conditions. We also explore how inferred molecular gas conditions depend on the assumptions made through the gas modeling approach.

2 Observations

The M82 galaxy is a prime target for molecular gas studies because it is nearby (D = 3.5 Mpc) and bright, making fainter emission detectable [18]. Notably, M82 has an enhanced star formation rate (SFR) of 13 $M_\odot$ per year, compared to the Milky Way Galaxy's 1.7 $M_\odot$ per year [19]. See Appendix A.1 for a quantitative visualization of M82's SFR.

2.1 Data

The CO isotopologue transitions emit photons at millimeter and sub-millimeter wavelengths, making emission observable by radio and far-infrared telescopes. We obtain high resolution data of six lines from the Submillimeter Array (SMA) in Hawaii and the Northern Extended Millimeter Array (NOEMA) in France. We summarize the individual observations, which cover different spatial scales with varying angular and spectral resolution, in Table 1,

Table 1: Summary of CO lines, including telescope, energy transition, emission frequency, and angular and spectral resolution.

Telescope	Line	Rest Frequency (GHz)	Beam Size ($''$)	Physical Scale (pc)	Spec. Resolution (km/s)
NOEMA	$C^{18}O$ $J = 1$–0	109.782	2.2	40	20
NOEMA	^{13}CO $J = 1$–0	110.201	2.2	40	20
NOEMA	CO $J = 1$–0	115.271	2.1	38	5
SMA	$C^{18}O$ $J = 2$–1	219.560	4.7	85	5
SMA	^{13}CO $J = 2$–1	220.399	4.2	76	5
SMA	CO $J = 2$–1	230.538	3.5	63	5

To homogenize and combine the observations, we use the `PyStructure`[2] script. More detailed descriptions on the data processing are outlined in [20]. We convolve observations to a common angular resolution of 4.7" set by the $C^{18}O$ (2–1) line. With this resolution, we can resolve a physical distance of 85 pc. Giant molecular clouds are $\sim 10^2$ pc in diameter, and thus our observations allow us to see trends on the star-forming molecular cloud scale [21]. `PyStructure` also derives so-called "moments" for each sightline, which allow us to quantify emission. Moment 0 is the velocity-integrated brightness temperature, also known as the intensity of emission, and moment 2 is the estimated velocity dispersion, or the width of the emission line.

[2] `https://github.com/jdenbrok/PyStructure/`

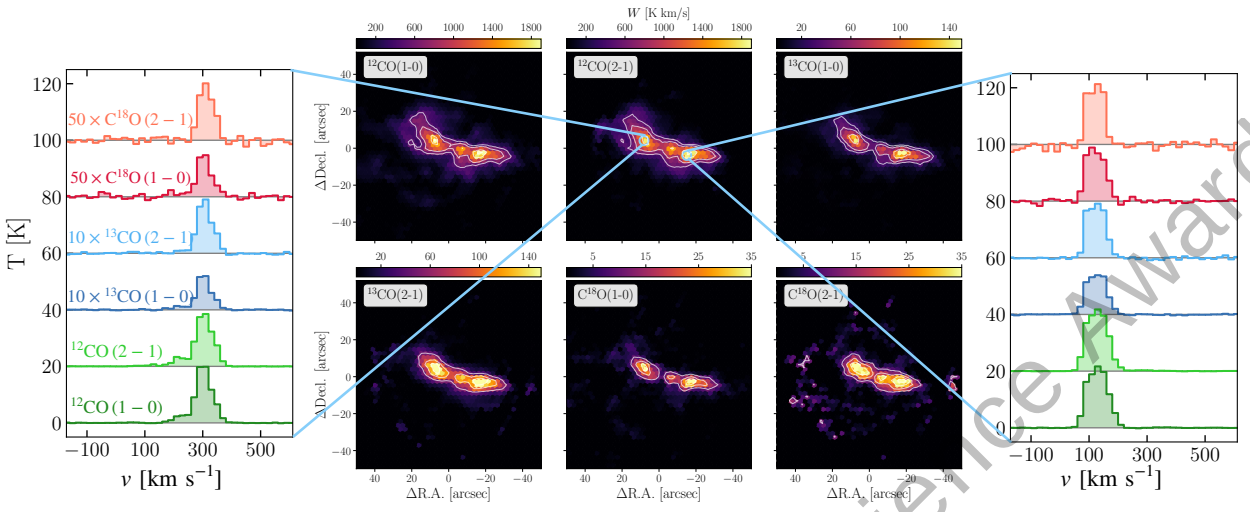

Figure 1: CO Isotopologue Emission and Moment 0. The panels in the middle show the (1–0) and (2–1) energy transitions from each of the isotopologues ^{12}CO, ^{13}CO, and C^{18}O. We also plot emission spectra for two pixels in the center regions of the galaxy. Note that we scale emission from ^{13}CO and C^{18}O for visibility purposes.

The resulting homogenized data includes the emission spectrum and moment maps. In Figure 1, we present the moment-0 maps from all lines. We also highlight two lines of sight in the center of the galaxy and plot their corresponding spectra.

3 Methods

We consider two models of emitting molecular gas. First, following the common approach in literature, we assume that the conditions of emitting gas in each line of sight (also referred to as pixel or sightline, these phrases refer to the smallest, resolvable region of gas ∼85 pc) is uniform. Next, in effort to more accurately describe the gas, we implement a model that assumes the density of gas in each sightline is smoothly changing with varying widths. With these approaches to emitting gas, we then simulate the intensities of CO isotopologue transitions.

3.1 Solving the non-LTE Radiative Transfer Equations

The non-LTE radiative transfer simulation RADEX allows us to model observed line intensities from ^{12}CO, ^{13}CO, and C^{18}O under various environmental conditions. RADEX assumes homogeneous gas and solves the radiative transfer equations to find a converged solution for the level population (see Appendix A.2 for more details). Importantly, RADEX allows us to compare simulated emission to observed emission, thereby enabling us to fit for the molecular gas conditions. We use molecular data files from the Leiden Atomic and Molecular Database [22], and we assume the CO isotopologues only collides with H_2 because H_2 is much more abundant than any other molecule ($[^{12}CO/H_2] \sim 10^{-4}$) [3].

3.2 Uniform Density Model

We first simulate emitting gas by assuming uniform conditions in a sightline. While this assumption may oversimplify the gas conditions, this approach is more straightforward and offers us a heuristic for gas modeling.

Under this assumption, the parameters governing each line of sight include the density of H_2 (n_{H_2}), kinetic temperature (T_{kin}), CO column density (N_{CO}), the abundance ratio between ^{12}CO and ^{13}CO ($X_{12/13}$), the abundance ratio between ^{13}CO and C^{18}O ($X_{13/18}$), and finally, the beam filling factor (Φ) [3]. The conditions listed are all relevant to describing the molecular gas characteristics in relation to star formation: H_2 and T_{kin} are analogs to how excited the gas is and N_{CO} can be translated into how much total gas there is. The relative amounts of CO isotopologue are influenced and driven by star formation, and thus the abundance ratios can give insight into the process. The Φ parameter is constrained for in effort to model the gas more accurately: we introduce Φ to account for the clumpy and

[3] Φ characterises the fraction of the spatial resolution element (the beam) that is covered by the source. For an unresolved source, only a portion of the beam will be "filled" by emission from the source. As a consequence, we measure a lower flux density, as the emission gets diluted over the beam area.

filamentary nature of the molecular ISM. We assume Φ is the same for all lines and account for Φ by directly multiplying the simulated intensity by Φ.

We run RADEX by creating a 6D grid with the grid-points iterating through a range for each parameter. The range and step size of each parameter is outlined in Table 2 (note this table outlines ranges for both models), and these ranges and step sizes are chosen based off of previous studies of similar environments [9]. Our grid is roughly 12.4 million parameter sets, meaning for each line of sight, we consider 12.4 million different parameter sets to describe the gas. This is comparable to the 30 million sets considered in [9].

Table 2: Summary of Gas Phase Initial Conditions for Both Models

Model Prescription	Parameter	Range	Stepsize
Both Models	$\log_{10}(n_{\mathrm{H_2}}\,[\mathrm{cm^{-3}}])$	2.0 – 5.0	0.2 dex
	$\log_{10}(\mathrm{T_{kin}}\,[\mathrm{K}])$	0.6 – 2.2	0.1 dex
	$\log_{10}(N_{\mathrm{CO}}\,[\mathrm{cm^{-2}}])$	16.0 – 19.0	0.2 dex
	$\mathrm{X_{12/13}}$	10 – 200	10
	$\mathrm{X_{13/18}}$	2 – 20	1.5
	$\Delta v\,[\mathrm{kms^{-1}}]$	10	...
Uniform	$\log_{10}(\Phi)$	-2 – 0	0.2 dex
Log-normal	σ	0.2 – 1	0.1

3.3 Implementing a Sophisticated Changing Gas Phase

Theoretical and observational studies have shown that molecular clouds have a range of H_2 gas densities, and can not necessarily be described by a uniform density, as assumed in our "uniform" model [23]. In an effort to model the molecular gas more physically and therefore more accurately, we implement a log-normal distribution for the density of H_2. The log-normal distribution assumption follows from literature, which analyzed high resolution observations of CO molecular cloud emission [24]. This form of gas modeling has not been

employed readily in current research. Following formulations modeling the density of a cloud, we adopt the probability density function (PDF) method used in [25]. The gas density in a molecular cloud is described by

$$d\mathrm{P}\left(\ln n'\right) \propto \exp\left(-\frac{(\ln n' - \overline{\ln n'})^2}{2\sigma^2}\right) d\left(\ln n'\right), \tag{1}$$

where dP is the fraction of molecules with volume densities in a logarithmic step $d\ln n'$ centered on n', $n' = n_{\mathrm{H_2}}/n_0$ is the volume density normalized by the mean volume density, n_0, and σ is the width of the distribution [4]. Refer to Appendix A.3 for visualization of log-normal distributions.

Under this model, the parameters governing each line of sight include $n_{\mathrm{H_2}}, \mathrm{T_{kin}}, N_{\mathrm{CO}}, X_{12/13}, X_{13/18}$ and σ, the width of the log-normal distribution. We do not consider Φ in this model because we account for the fact that the entire beam is not fully filled with the gas at the density at which it will emit efficiently. As we also include low density gas within our model (i.e. gas which will not effectively emit), our derived parameters are already beam averaged.

We implement the density distribution by building on the modeled RADEX grid. The adjusted intensities correspond to the sum of intensities weighted by the density PDF as follows:

$$\mathrm{I} = \frac{\int n_{\mathrm{H_2}} P\left(n_{\mathrm{H_2}}\right) \mathrm{I}\left(n_{\mathrm{H_2}}, N_{\mathrm{CO}}, \mathrm{T_{kin}}, X_{12/13}, X_{13/18}\right)\, dn_{\mathrm{H_2}}}{\int n_{\mathrm{H_2}} P\left(n_{\mathrm{H_2}}\right) dn_{\mathrm{H_2}}}. \tag{2}$$

3.4 Fitting Modeled to Observed with RADEX

For both approaches, we infer the conditions by finding the parameter set out of around 12 million for which the model intensities best matches the observed. We adopt the maximum likelihood analysis outlined in [9]. On a pixel by pixel basis, we look at each hypothesized set of parameters $\theta = (n_{\mathrm{H_2}}, \mathrm{T_{kin}}, N_{\mathrm{CO}}, X_{12/13}, X_{13/18}, \Phi)$ or σ depending on the model, and

[4] Note that the distribution does not peak at the center volume density (n_0), but rather it peaks at $\overline{\ln n'}$.

we evaluate the quality of fit with the χ^2 test. We have

$$\chi^2(\theta) = \sum_{i=1}^{n} \left(\frac{I_i^{\rm model}(\theta) - c_i^{\rm line} \cdot I_i^{\rm obs}}{\sigma_i^{\rm obs}} \right)^2, \tag{3}$$

where $c_i^{\rm line}$ considers the adjustment of the line width. We use $c_i^{\rm line} = 10\,{\rm km\,s^{-1}}/{\rm FWHM_i}$, where the FWHM is the derived moment-2 value (see Section 2.1). We consider contributions from all 6 lines, so $n = 6$. The terms $I_i^{\rm model}$ and $I_i^{\rm obs}$ represent the modeled and observed intensity of the i-th line, respectively. The parameter σ_i is the observational uncertainty and should not to be confused with the distribution width σ. We translate from χ^2 to a probability by assuming a multivariate Gaussian probability distribution, with

$$P(I^{\rm obs}|\theta) = \left(\prod_i^n (2\pi\sigma_i^2)^{-\frac{1}{2}} \right) \cdot e^{-\frac{1}{2}\chi^2(\theta)}. \tag{4}$$

After calculating the probability corresponding to every parameter set θ, we end with a 6D probability cube. We then perform marginalization for each parameter by summing the likelihood over the full range of parameters except the one(s) in question. The resulting "1DMax solution" parameter is then selected by determining the highest 1D likelihood in each parameter. For details, see [9].

3.5 Calculating the CO-to-H_2 Conversion Factor

This paper also studies the value and trends of the CO-to-H_2 conversion factor ($\alpha_{\rm CO}$), which is the ratio between H_2 column density and the integrated intensity of ^{12}CO 1–0. CO constitutes the most accessible tracer of molecular gas in extragalactic studies, so this conversion factor is crucial for much of current astrophysics research. It can be expressed as a function of $N_{\rm CO}$, Φ, and the CO 1–0 intensity $I_{\rm CO(1-0)}$ by

$$\alpha_{\rm CO} = \frac{M_{\rm mol}}{L_{\rm CO(1\text{-}0)}} \left[\frac{M_\odot}{\rm K\ km\ s^{-1}\ pc^2} \right] = \frac{1}{4.5 \times 10^{19}} \cdot \frac{N_{\rm CO}\,[{\rm cm^{-2}}]\,\Phi}{x_{\rm CO}\,I_{\rm CO(1\text{-}0)}\,[{\rm K\ km\ s^{-1}}]}, \tag{5}$$

where $x_{\rm CO}$ is the CO/H_2 abundance ratio.

Our modeling from the uniform model directly constrains $N_{\rm CO}$ and Φ and provides a simulated $I_{\rm CO(1-0)}$ value, and thus we can derive the spatial distribution of $\alpha_{\rm CO}$. We note we did not constrain for $x_{\rm CO}$, which requires more extensive observations. We assume $x_{\rm CO} =$

3×10^{-4}, which is supported by values found in star-forming clouds and commonly adopted in literature for starburst environments [26, 27, 28]. Since the motivation for Φ is implicitly included in our log-normal density model, as explained in Section 3.3, we set $\Phi = 1$.

4 Results and Analysis

4.1 Uniform vs. Log-normal Model

From our derived distributions for each sightline, we can construct "corner plots" which visualize the results. In Figure 2, we present a corner plot derived from a sightline in the center of the galaxy. On the left and in red is that from the uniform gas model, and on the right and in blue is that from the log-normal density model (for the rest of this paper, red corresponds to the uniform model and blue corresponds to the log-normal model). The vertical line on the PDFs along the 1D distributions is the 1DMax solution. The statistics of the 1DMax solutions are listed in Table 3, some of which are further discussed in Section 5. Overall, we find that our marginalized PDFs for the parameters are generally single-peaked, indicating we do not run into any strong degeneracies. In both corner plots, $X_{12/13}$ and $N_{\rm CO}$ appear to be the most well constrained, while $X_{13/18}$ is the least well constrained.

In Figure 3, we plot the fits of parameters shared between the models, which include $X_{12/13}, X_{13/18}, N_{\rm CO}$, $\rm T_{kin}$, and $n_{\rm H_2}$. We make two notes: first, because we consider the Φ in our uniform model, the $N_{\rm CO}$ value we constrain is the sub-beam value, i.e the $N_{\rm CO}$ in the smaller beam. In Figure 3, we convert from sub-beam to full-beam $N_{\rm CO}$ by multiplying by Φ. Second, our $n_{\rm H_2}$ values from the two models are not directly comparable because for the log-normal model, $n_{\rm H_2}$ is the average density rather than the sole density. Nonetheless, it is still instructive to visually assess their distributions.

The histograms are the distribution of the 1DMax solutions, the dotted vertical lines are the medians of the 1DMax solutions over all pixels, and the horizontal markers at the

Table 3: Statistics for 1DMax solutions across all pixels. We list the median, mean, and standard deviation of the derived 1DMax parameters.

Model		$\log(n_{H_2})$ $[cm^{-3}]$	$\log T_{kin}$ [K]	$\log N_{CO}$ $[cm^{-2}]$	$X_{12/13}$	$X_{13/18}$	$\log \Phi$	σ
Uniform	Median	3.71	1.4	18.2	60.0	5.0	0.4	–
	Mean	3.4	1.65	18.46	74.84	5.3	0.59	–
	Std. Dev.	0.42	0.32	0.43	42.51	2.71	0.27	–
Log-normal Density	Median	4.2	1.3	17.80	60.0	3.5	–	0.4
	Mean	4.3	1.33	17.93	70.21	3.89	–	0.50
	Std. Dev.	0.56	0.19	0.44	46.07	2.63	–	0.35
Comparison	p-value	$\ll 0.05$	$\ll 0.05$	$\ll 0.05$	>0.05	$\ll 0.05$	–	–

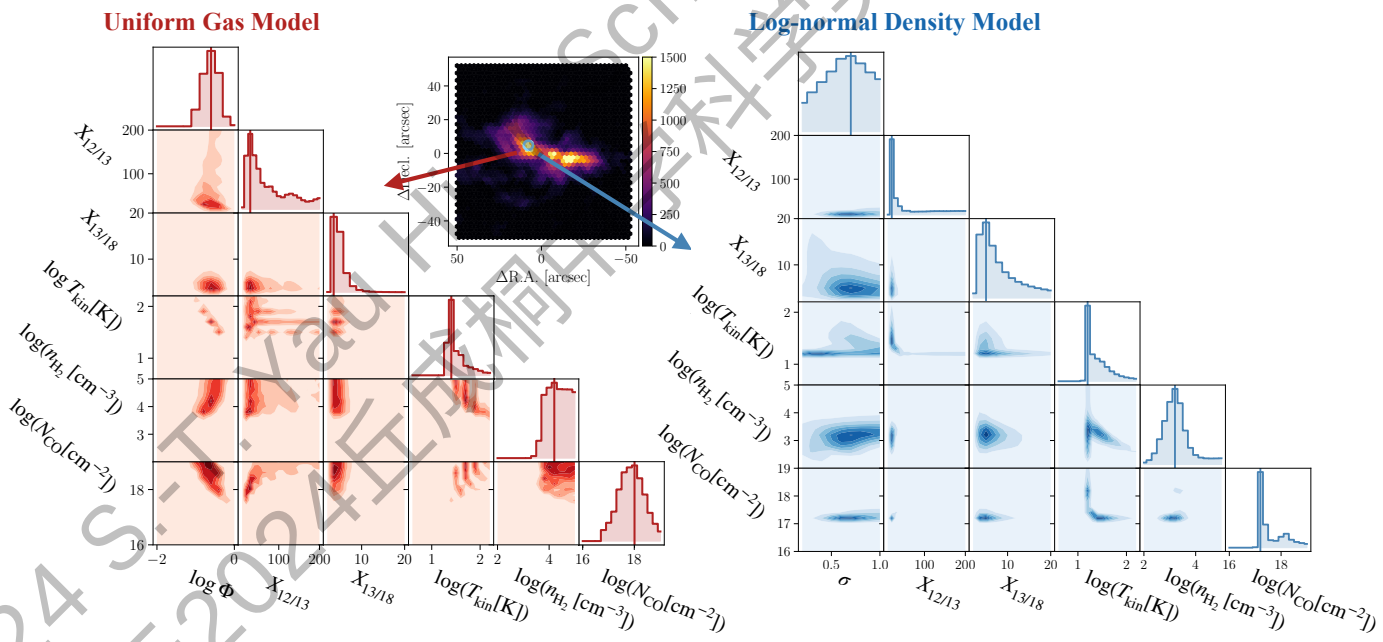

Figure 2: Marginalized 1D and 2D likelihood distributions from a bright central pixel. The red (left) corner plot is derived from our uniform model, and the blue (right) corner plot is derived from our log-normal model. The map in the middle depicts the integrated intensity with one sightline circled from which the two corner plots are generated.

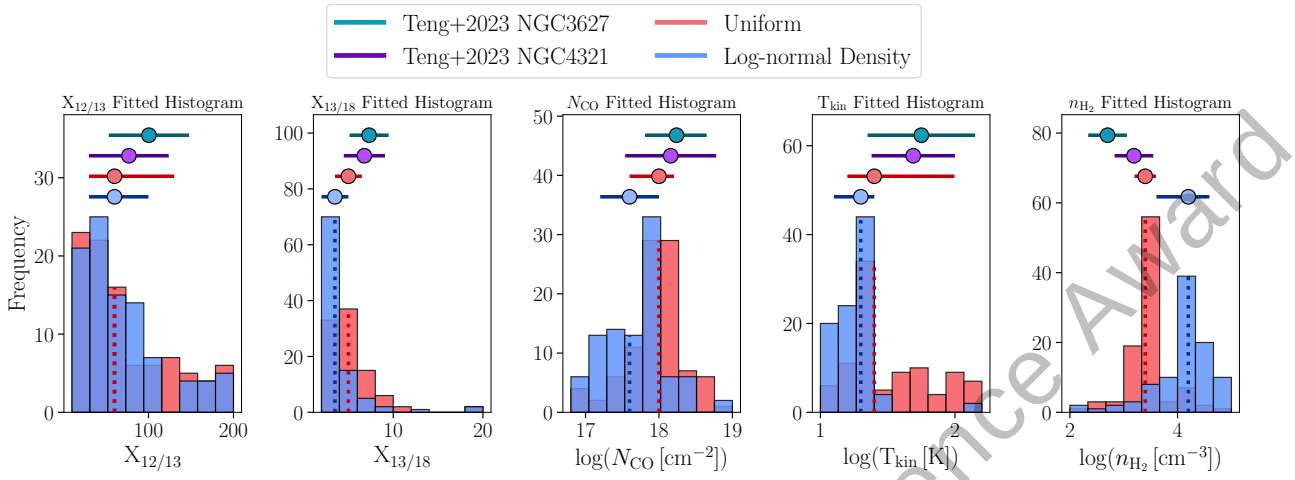

Figure 3: Distributions of 1DMax fitted parameters for $X_{12/13}, X_{13/18}, N_{\rm CO}, {\rm T_{kin}}$, and $n_{\rm H_2}$ from both models. We plot histograms of 1DMax fitted parameters, with the uniform model in red and the log-normal density model in blue. The vertical dotted line is the median of the 1DMax values. In the horizontal markers above, we plot the weighted $16^{\rm th}$-to-$84^{\rm th}$ percentile range from our results and from results found in [29] for similar starburst galaxy centers.

top of the plots indicate the weighted $16^{\rm th}$-to-$84^{\rm th}$ percentile range. Above our fits, we show values found in the centers of NGC 3627 and NGC 4321, which are similar nearby starburst galaxies [29]. We see the two models generally agree for the medians of the $X_{12/13}$, $X_{13/18}$, and $\rm T_{kin}$ parameters. However, the width of the distribution of $\rm T_{kin}$ from the Uniform model is wider. For the $N_{\rm CO}$ parameter, the models are systematically offset from one another by 0.2 dex. Generally, the conditions found by [29] are more extreme than ours.

From Table 3, we see our analysis yields high $\rm T_{kin}$ and $n_{\rm H_2}$, with mean $\rm T_{kin}$ and $n_{\rm H_2}$ exceeding 100 K and 5×10^3 cm $^{-3}$ respectively. The derived $X_{13/18}$ values across the center are lower than the Galactic Center value, which is between 6 and 8 [30]. On the other hand, our inferred $X_{12/13}$ values are higher than the $X_{12/13} \sim 25$ of Galactic Center [31]. The smaller $X_{13/18}$ value may indicate $\rm C^{18}O$ enrichment from enhanced star formation. The higher $X_{12/13}$ values align with values found in other starburst galaxy centers, which range from ~ 40 to > 100. These enhanced values are likely a result of higher inflow rates and stellar nucleosynthesis enrichment, and shed light on traces left by star formation [32, 28].

We finally compare our derived values to those found in literature for the M82 galaxy. However, we note that previous studies of M82 do not resolve the galaxy on cloud scale, and some do not employ non-LTE modeling. Our work is the first to combine non-LTE studies with high resolution data. In [33], Ward obtained high J rotational lines of ^{12}CO and derived $N_{\rm CO}$ between $10^{17.1}$ and $10^{18.8}$ cm $^{-2}$, which is within the scatter of our models. In [34], Weiss explained excitation of transitions beyond the $J = 4$–3 transition arise from gas likely with $\log n_{\rm H_2} \sim 3.5 - 4.5$ cm $^{-3}$ and $\log {\rm T_{kin}} \geq 1.6$. We find $n_{\rm H_2}$ values within the range, but the log-normal derived $\rm T_{kin}$ drop below. We emphasize that our results provide a much smaller range than those currently in literature. We discuss further in Section 5.

4.2 The CO-to-H_2 Conversion Factor

The CO-to-H_2 conversion factor $\alpha_{\rm CO}$ is vital to studying molecular gas and star formation, and its value is critical to ongoing astrophysics research. With Equation 5, we compute $\alpha_{\rm CO}$ on a pixel by pixel basis. We then compute the average $\alpha_{\rm CO}$ for each pixel by weighting the derived $\alpha_{\rm CO}$ for the grid-points by the corresponding normalized probability calculated with Equation 4. This yields the inferred $\alpha_{\rm CO}$ for each pixel in the M82 center. We find $\alpha_{\rm CO} = 0.64 \pm 0.22$ from our uniform model and $\alpha_{\rm CO} = 0.41 \pm 0.24\, M_\odot\, {\rm pc}^{-2}/({\rm K\,km\,s^{-1}})$ from our log-normal density model. Our results show that all pixels in the galaxy center have $\alpha_{\rm CO}$ 4–11 times lower than the Galactic Center average of 4.4. Our findings match lower values found in other galaxy centers using independent techniques [35, 36].

Analyzing how $\alpha_{\rm CO}$ relates with environmental conditions and observational tracers is crucial to understanding star formation. Previous literature suggests that the ^{12}CO/^{13}CO 2–1 ratio (the ratio between $\rm I_{^{12}CO(2-1)}$ and $\rm I_{^{13}CO(2-1)}$) is an observational tracer of $\alpha_{\rm CO}$. This correlation is expected: because ^{12}CO is optically thick whereas ^{13}CO is optically thin, the intensity ratio inversely traces optical depth. Optical depth variations are then directly related to $\alpha_{\rm CO}$: the more optically thick, the higher $\alpha_{\rm CO}$ because less CO emission is observed.

We investigate this correlation in Figure 4. We plot our derived $\alpha_{\rm CO}$ against the $\log {\rm CO}/^{13}{\rm CO}$ (2–1) ratio, and we overplot the trend found in [29] for the NGC 3627 and NGC 4321 galaxies. We sort the data into 4 bins, average the $\alpha_{\rm CO}$ in each bin, and plot the corresponding data points as stars. Our log-normal trend follows [29] less closely, but we note that the binned trend for the third bin is driven by few points, and we are heavily limited in dynamical range. However, our findings still reinforce the suggestion that [29] makes: the ${\rm CO}/^{13}{\rm CO}$ $(2-1)$ ratio can be used as an observational tracer for $\alpha_{\rm CO}$.

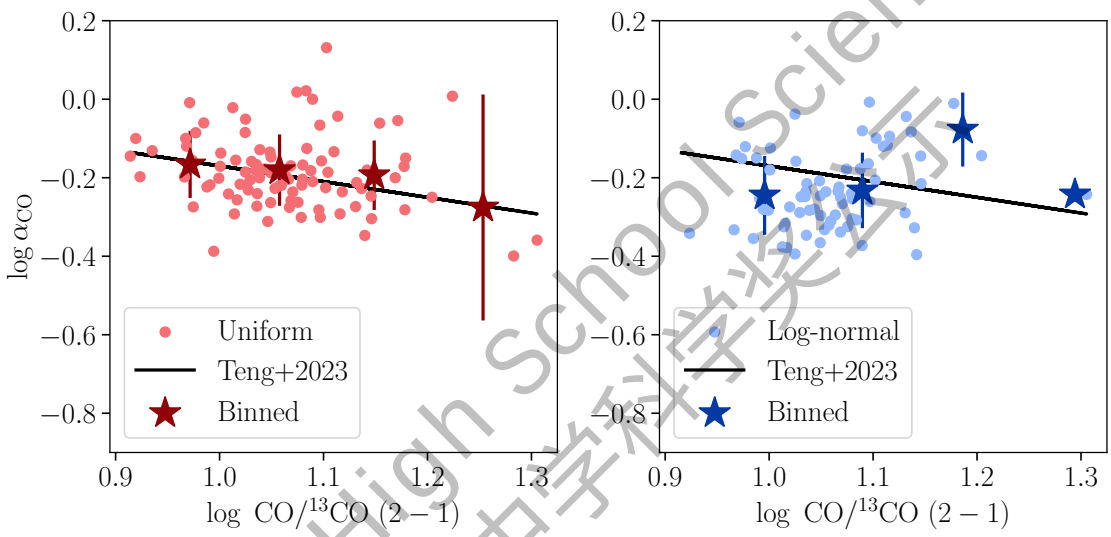

Figure 4: Relation of the modeled $\log \alpha_{\rm CO}$ with the observed $\log {}^{12}{\rm CO}/^{13}{\rm CO}$ 2–1 line ratio. We average the points in 4 bins and plot them as stars. The black line is the power law relation found by [29]. Despite a $\sim$0.2 dex scatter in both relations, there is a clear trend of $\log \alpha_{\rm CO}$ decreasing with the line ratio, suggesting these observable properties as potential tracers for $\log \alpha_{\rm CO}$ variations in starburst galaxy centers.

5 Discussion

Our work considers how the gas-modeling method impacts derived molecular conditions. To quantify the difference in our results from our two models, we perform the two-sample Kolmogorov-Smirnov (KS) test to the fitted parameter distributions. We list the derived p-values in Table 3. The p-values, with the exception of $X_{12/13}$, are less than 0.05. The KS

test quantitatively suggests the derived distributions are significantly different.

Looking to Figure 3, we see that the log-normal model derives a lower T_{kin} but higher n_{H_2}. These parameters define the excitation conditions of the clouds, and a degeneracy does exist between them. This degeneracy was also alluded to in our comparison to literature values. Resolving this degeneracy requires higher $-J$ CO transitions or obtaining another observational tracer to further constrain T_{kin} or n_{H_2}.

We also compute the CO-to-H_2 conversion factor assuming a x_{CO} value. Our results emphasize the ability of CO/^{13}CO $(2-1)$ to act as an observational tracer for α_{CO}. We note that changes in x_{CO} may impact the derived α_{CO}. However, our modeling cannot constrain the x_{CO} values, and we leave this question open.

Our results on the molecular gas conditions in M82 are much more tightly constrained than those reported in the existing literature. However, the discrepancies in our derived results between models raises questions of how astronomers should build sophisticated models of molecular gas. Examples of such models include those that iterate the x_{CO} ratio or account for a changing T_{kin}. With our current data, we are unable to implement these models because of limitations with degrees of freedom: with 6 lines, we can fit for at most 6 parameters.

6 Conclusion

We present a high resolution CO isotopologue analysis across the center of the M82 galaxy. We model molecular emission under two models: a uniform and a log-normal approach. We use these models together with non-LTE radiative transfer simulations and likelihood analysis to constrain the properties of the star-forming gas within the galaxy. From our derived parameters, we compute the CO-to-H_2 conversion factor, α_{CO}, which translates from observations to the mass of star-forming reservoirs. Our main findings are as follows:

- We derived a total of seven critical gas properties with much less uncertainty than

current literature. Our results align with values derived for similar environments.

- We found that the derived parameters from our two models differ significantly through the KS test. This result highlights the need for astronomers to carefully consider approaches to gas modeling. As instrumental design improves, it is crucial for the development of sophisticated models to follow.

- We found a direct correlation between ^{12}CO/^{13}CO (2–1) intensity ratio and $\alpha_{\rm CO}$, a critical value in astrophysical research. This result reveals that we can use ^{12}CO/^{13}CO (2–1) as an observational tracer for the $\alpha_{\rm CO}$ value in similar starburst environments, meaning we can use the observed ratio as a direct way to calculate $\alpha_{\rm CO}$, thus avoiding complicated and expensive analysis. This result also motivates further research on other possible tracers.

Analyzing star-forming molecular gas is crucial to understanding how stars form, and in this work, we relate molecular gas conditions to possible physical explanations. We emphasize the need for caution and robust modeling of CO emission to keep pace with advancements in instrumentation and observation. As higher quality and larger volumes of data become available, astronomers must continue developing and testing sophisticated models. In future work, it is critical to obtain more CO isotopologue emission (higher $-J$, or other isotopologues) or consider emission from other molecules such as HCO+ and HCN+.

7 Key Takeaways

The methods and two models we use in this study inferred the properties of molecular gas in the galaxy M82 to much less uncertainty than the previous literature, and their applicability is not limited to just M82. Their paradigms can be adopted for other contexts when modeling molecular gas, and the results derived from these models can help inform

star formation at large. We found an observational tracer for the observational tracer for the CO-to-H_2 factor, a critical value in current astronomy research. This finding means that astronomers can directly trace the conversion factor and avoid complicated and expensive analysis.

8 Acknowledgments

To my mentor Dr. Jakob den Brok, thank you for your unwavering guidance and kindness. To my PI Dr. Qizhou Zhang, thank you for your support and for welcoming me back to your group. To the Harvard & Smithsonian Center for Astrophysics, thank you for hosting me.

I am in debt of gratitude for the Center for Excellence in Education, its Research Science Institute, and the Massachusetts Institute of Technology for providing me the opportunity to conduct this research. Thank you to the sponsors of CEE for making this entire experience possible. I am beyond grateful for the support I have received throughout this research.

References

[1] C. F. McKee and E. C. Ostriker. Theory of Star Formation. *ARA&A*, 45(1):565–687, Sept. 2007.

[2] R. C. Kennicutt and N. J. Evans. Star Formation in the Milky Way and Nearby Galaxies. *ARA&A*, 50:531–608, Sept. 2012.

[3] J. S. den Brok. *Unraveling Molecular Gas Conditions across Nearby Galaxies with CO Isotopologues*. PhD thesis, Uni Bonn, 2022.

[4] E. Schinnerer and A. K. Leroy. Molecular Gas and the Star Formation Process on Cloud Scales in Nearby Galaxies. *arXiv e-prints*, page arXiv:2403.19843, Mar. 2024.

[5] A. A. Kepley, A. K. Leroy, D. T. Frayer, A. Usero, J. Marvil, and F. Walter. The Green Bank Telescope Maps the Dense Molecular Gas in the Starburst Galaxy M82. In *American Astronomical Society Meeting Abstracts #223*, volume 223 of *American Astronomical Society Meeting Abstracts*, page 244.05, Jan. 2014.

[6] A. Heiderman, I. Evans, Neal J., L. E. Allen, T. Huard, and M. Heyer. The Star Formation Rate and Gas Surface Density Relation in the Milky Way: Implications for Extragalactic Studies. *ApJ*, 723(2):1019–1037, Nov. 2010.

[7] M. J. Jiménez-Donaire, F. Bigiel, A. K. Leroy, A. Usero, D. Cormier, J. Puschnig, M. Gallagher, A. Kepley, A. Bolatto, S. García-Burillo, A. Hughes, C. Kramer, J. Pety, E. Schinnerer, A. Schruba, K. Schuster, and F. Walter. EMPIRE: The IRAM 30 m Dense Gas Survey of Nearby Galaxies. *ApJ*, 880(2):127, Aug. 2019.

[8] P. Madau and M. Dickinson. Cosmic Star-Formation History. *ARA&A*, 52:415–486, Aug. 2014.

[9] Y.-H. Teng, K. M. Sandstrom, J. Sun, A. K. Leroy, L. C. Johnson, A. D. Bolatto, J. M. D. Kruijssen, A. Schruba, A. Usero, A. T. Barnes, F. Bigiel, G. A. Blanc, B. Groves, F. P. Israel, D. Liu, E. Rosolowsky, E. Schinnerer, J. D. Smith, and F. Walter. Molecular Gas Properties and CO-to-H_2 Conversion Factors in the Central Kiloparsec of NGC 3351. *ApJ*, 925(1):72, Jan. 2022.

[10] I. Dabrowski. The Lyman and Werner bands of H_2. *Canadian Journal of Physics*, 62:1639, Dec. 1984.

[11] A. D. Bolatto, M. Wolfire, and A. K. Leroy. The CO-to-H_2 Conversion Factor. *ARA&A*, 51(1):207–268, Aug. 2013.

[12] R. Shetty, S. C. Glover, C. P. Dullemond, E. C. Ostriker, A. I. Harris, and R. S. Klessen. Modelling CO emission - II. The physical characteristics that determine the X factor in Galactic molecular clouds. *MNRAS*, 415(4):3253–3274, Aug. 2011.

[13] W. D. Langer and A. A. Penzias. 12C/ 13C Isotope Ratio across the Galaxy from Observations of 13C 18O in Molecular Clouds. *ApJ*, 357:477, July 1990.

[14] J. G. A. Wouterloot, C. Henkel, J. Brand, and G. R. Davis. Galactic interstellar $^{18}O/\{\hat{1}7\}O$ ratios - a radial gradient? *A&A*, 487(1):237–246, Aug. 2008.

[15] T. L. Wilson, K. Rohlfs, and S. Hüttemeister. *Tools of Radio Astronomy*. Springer, 2009.

[16] J. den Brok. In prep, CO isotopologue-derived molecular gas conditions and CO-to-H_2 conversion factors across M51. *ApJ*, 2024.

[17] Y. L. Shirley. The Critical Density and the Effective Excitation Density of Commonly Observed Molecular Dense Gas Tracers. *PASP*, 127(949):299, Mar. 2015.

[18] S. Lianou, P. Barmby, A. A. Mosenkov, M. Lehnert, and O. Karczewski. Dust properties and star formation of approximately a thousand local galaxies. *A&A*, 631:A38, Nov. 2019.

[19] Y. Sofue. Is M82 a Disk-Truncated Bulge by a Close Encouter with M81? *PASJ*, 50:227–231, Apr. 1998.

[20] J. S. den Brok, F. Bigiel, K. Sliwa, T. Saito, A. Usero, E. Schinnerer, A. K. Leroy, M. J. Jiménez-Donaire, E. Rosolowsky, A. T. Barnes, J. Puschnig, J. Pety, A. Schruba, I. Bešlić, Y. Cao, C. Eibensteiner, S. C. O. Glover, R. S. Klessen, J. M. D. Kruijssen, S. E. Meidt, L. Neumann, N. Tomičić, H.-A. Pan, M. Querejeta, E. Watkins, T. G. Williams, and D. Wilner. A CO isotopologue Line Atlas within the Whirlpool galaxy Survey (CLAWS). *A&A*, 662:A89, June 2022.

[21] A. D. Bolatto, A. K. Leroy, E. Rosolowsky, F. Walter, and L. Blitz. The Resolved Properties of Extragalactic Giant Molecular Clouds. *ApJ*, 686(2):948–965, Oct. 2008.

[22] F. L. Schöier, F. F. S. van der Tak, E. F. van Dishoeck, and J. H. Black. An atomic and molecular database for analysis of submillimetre line observations. *A&A*, 432(1):369–379, Mar. 2005.

[23] A. Nishimura, K. Tokuda, K. Kimura, K. Muraoka, H. Maezawa, H. Ogawa, K. Dobashi, T. Shimoikura, A. Mizuno, Y. Fukui, and T. Onishi. Revealing the Physical Properties of Molecular Gas in Orion with a Large-scale Survey in J = 2-1 Lines of ^{12}CO, ^{13}CO, and $C^{18}O$. *ApJS*, 216(1):18, Jan. 2015.

[24] A. Hughes, S. E. Meidt, E. Schinnerer, D. Colombo, J. Pety, A. K. Leroy, C. L. Dobbs, S. García-Burillo, T. A. Thompson, G. Dumas, K. F. Schuster, and C. Kramer. Probability Distribution Functions of $^{12}CO(J = 1 \rightarrow 0)$ Brightness and Integrated Intensity in M51: The PAWS View. *ApJ*, 779(1):44, Dec. 2013.

[25] A. K. Leroy, A. Usero, A. Schruba, F. Bigiel, J. M. D. Kruijssen, A. Kepley, G. A. Blanc, A. D. Bolatto, D. Cormier, M. Gallagher, A. Hughes, M. J. Jiménez-Donaire, E. Rosolowsky, and E. Schinnerer. Millimeter-wave Line Ratios and Sub-beam Volume Density Distributions. *ApJ*, 835(2):217, Feb. 2017.

[26] J. H. Lacy, R. Knacke, T. R. Geballe, and A. T. Tokunaga. Detection of Absorption by H 2 in Molecular Clouds: A Direct Measurement of the H 2:CO Ratio. *ApJ*, 428:L69, June 1994.

[27] U. J. Sofia, J. T. Lauroesch, D. M. Meyer, and S. I. B. Cartledge. Interstellar Carbon in Translucent Sight Lines. *ApJ*, 605(1):272–277, Apr. 2004.

[28] K. Sliwa, C. D. Wilson, D. Iono, A. Peck, and S. Matsushita. Around the Ring We Go: The Cold, Dense Ring of Molecular Gas in NGC 1614. *ApJ*, 796(1):L15, Nov. 2014.

[29] Y.-H. Teng, K. M. Sandstrom, J. Sun, M. Gong, A. D. Bolatto, I.-D. Chiang, A. K. Leroy, A. Usero, S. C. O. Glover, R. S. Klessen, D. Liu, M. Querejeta, E. Schinnerer, F. Bigiel, Y. Cao, M. Chevance, C. Eibensteiner, K. Grasha, F. P. Israel, E. J. Murphy, L. Neumann, H.-A. Pan, F. Pinna, M. C. Sormani, J. D. Smith, F. Walter, and T. G. Williams. The Physical Drivers and Observational Tracers of CO-to-H_2 Conversion Factor Variations in Nearby Barred Galaxy Centers. *ApJ*, 950(2):119, June 2023.

[30] M. B. Areal, S. Paron, M. Celis Peña, and M. E. Ortega. Exploring the $^{13}CO/C^{18}O$ abundance ratio towards Galactic young stellar objects and HII regions. *A&A*, 612:A117, May 2018.

[31] T. L. Wilson and R. Rood. Abundances in the Interstellar Medium. *ARA&A*, 32:191–226, Jan. 1994.

[32] C. Henkel, H. Asiri, Y. Ao, S. Aalto, A. L. R. Danielson, P. P. Papadopoulos, S. García-Burillo, R. Aladro, C. M. V. Impellizzeri, R. Mauersberger, S. Martín, and N. Harada. Carbon and oxygen isotope ratios in starburst galaxies: New data from NGC 253 and Mrk 231 and their implications. *A&A*, 565:A3, May 2014.

[33] J. S. Ward, J. Zmuidzinas, A. I. Harris, and K. G. Isaak. A ^{12}CO J=6-5 Map of M82: The Significance of Warm Molecular Gas. *ApJ*, 587(1):171–185, Apr. 2003.

[34] A. Weiß, F. Walter, and N. Z. Scoville. The spectral energy distribution of CO lines in M 82. *A&A*, 438(2):533–544, Aug. 2005.

[35] J. S. den Brok, F. Bigiel, J. Chastenet, K. Sandstrom, A. Leroy, A. Usero, E. Schinnerer, E. W. Rosolowsky, E. W. Koch, I.-D. Chiang, A. T. Barnes, J. Puschnig, T. Saito, I. Bešlić, M. Chevance, D. A. Dale, C. Eibensteiner, S. Glover, M. J. Jiménez-Donaire, Y.-H. Teng, and T. G. Williams. Wide-field CO isotopologue emission and the CO-to-H_2 factor across the nearby spiral galaxy M101. *A&A*, 676:A93, Aug. 2023.

[36] A. W. Strong, I. V. Moskalenko, and O. Reimer. A New Determination of the Extragalactic Diffuse Gamma-Ray Background from EGRET Data. *ApJ*, 613(2):956–961, Oct. 2004.

[37] M. R. Blanton, M. A. Bershady, and B. Abolfathi. Sloan Digital Sky Survey IV: Mapping the Milky Way, Nearby Galaxies, and the Distant Universe. *AJ*, 154(1):28, July 2017.

[38] J. Kollmeier, S. F. Anderson, G. A. Blanc, M. R. Blanton, K. R. Covey, J. Crane, N. Drory, P. M. Frinchaboy, C. S. Froning, J. A. Johnson, J. P. Kneib, K. Kreckel, A. Merloni, E. W. Pellegrini, R. W. Pogge, S. V. Ramirez, H. W. Rix, C. Sayres, J. Sánchez-Gallego, Y. Shen, A. Tkachenko, J. R. Trump, S. E. Tuttle, A. Weijmans, G. Zasowski, B. Barbuy, R. L. Beaton, M. Bergemann, J. J. Bochanski, W. N. Brandt, A. R. Casey, B. A. Cherinka, M. Eracleous, X. Fan, R. A. García, P. J. Green, S. Hekker, R. R. Lane, P. Longa-Peña, S. Mathur, A. Meza, I. Minchev, A. D. Myers, D. L. Nidever, C. Nitschelm, J. E. O'Connell, A. M. Price-Whelan, M. J. Raddick, G. Rossi, R. Sankrit, J. D. Simon, A. M. Stutz, Y. S. Ting, B. Trakhtenbrot, B. A. Weaver, C. N. A. Willmer, and D. H. Weinberg. SDSS-V Pioneering Panoptic Spectroscopy. In *Bulletin of the American Astronomical Society*, volume 51, page 274, Sept. 2019.

A Appendix

A.1 M82

In Figure 5, we plot SFR versus stellar mass of nearby galaxies from the Sloan Digital Sky Survey. M82 lies significantly above both the main sequence band and the Milky Way. We also include a Hubble image of M82, which depicts dramatic plumes of hydrogen blasting out from central regions of stellar birth.

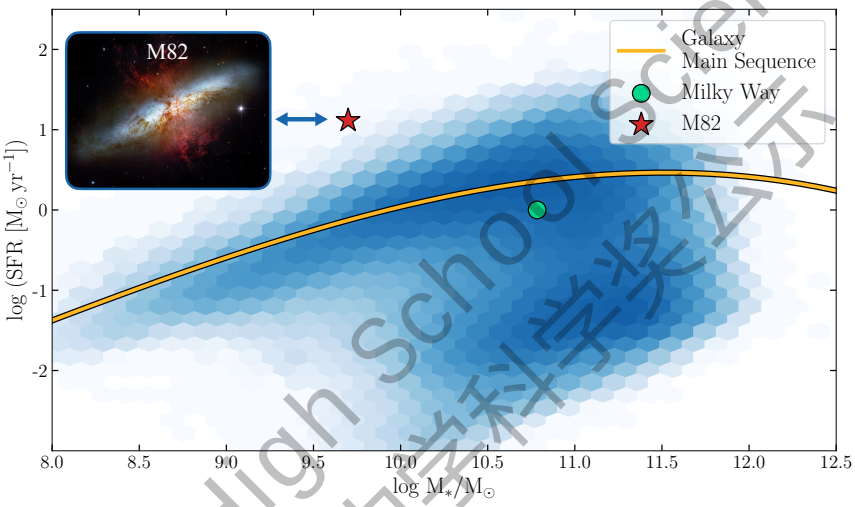

Figure 5: SFR Map of Nearby Galaxy Population. We highlight the main sequence galaxies with an orange band. The blue shaded histogram shows the distribution of nearby galaxy populations from SDSS. [37, 38].
Credit for M82 Inset: NASA, ESA and the Hubble Heritage Team (STScI/AURA). Acknowledgment: J. Gallagher (University of Wisconsin), M. Mountain (STScI) and P. Puxley (NSF).

A.2 RADEX

Behind the hood, RADEX is solving the radiative transfer equation, which governs how intensity I_ν changes as it propagates through a medium of path ds;

$$\frac{\mathrm{d}I_\nu}{\mathrm{d}s} = j_\nu - \kappa_\nu I_\nu. \tag{6}$$

In Equation 6, j_ν is the emission coefficient and describes the increase of radiation while κ_ν is the absorption coefficient and describes the decrease of radiation along the line of sight. These coefficients are governed by other values including the physical conditions of the gas, which we input to RADEX.

A.3 Log-normal Distribution

In Figure 6, we demonstrate the proposed gas density in a cloud with two distribution widths σ. Note that the y-axis is the $\log_{10}$ of the probability.

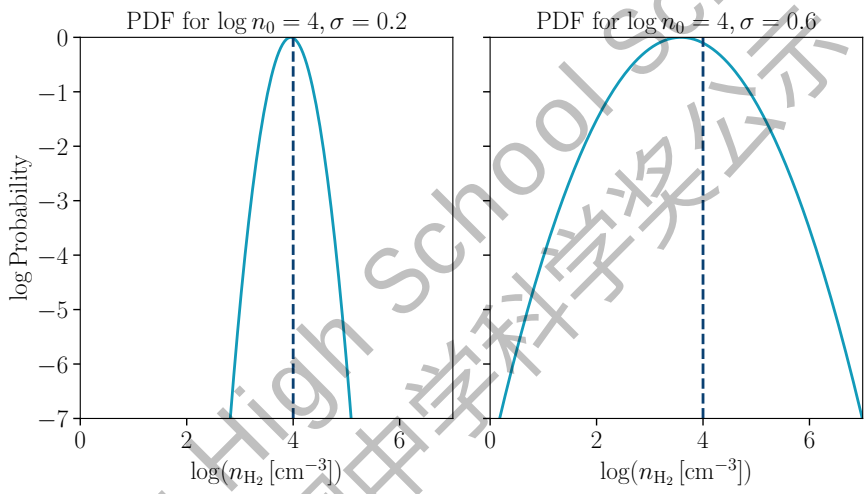

Figure 6: Log-normal density distribution. The panels demonstrate two examples of the PDF we implement for n_{H_2}. On the left, $\sigma = 0.2$; on the right, $\sigma = 0.6$, and in both plots, $\log n_0 = 4$.